JGR Space Physics

RESEARCH ARTICLE
10.1029/2022JA030616

Long-Term Variation of Lunar Semidiurnal Tides in the MLT Region Revealed by a Meteor Radar Chain

Jiahui Luo[1,2,3], Yun Gong[1,2,3], Zheng Ma[1,2,3], Shaodong Zhang[1,2,3,4,5], Qihou Zhou[6], Chunming Huang[2,3], Kaiming Huang[2,3], and Guozhu Li[7]

[1]Hubei Luojia Laboratory, Wuhan, China, [2]School of Electronic Information, Wuhan University, Wuhan, China, [3]Key Laboratory of Geospace Environment and Geodesy, Ministry of Education, Wuhan, China, [4]State Key Laboratory of Information Engineering in Surveying, Mapping and Remote Sensing, Wuhan University, Wuhan, China, [5]Guizhou Normal University, Guiyang, China, [6]Electrical and Computer Engineering Department, Miami University, Oxford, OH, USA, [7]Key Laboratory of Earth and Planetary Physics, Chinese Academy of Sciences, Institute of Geology and Geophysics, Beijing, China

Key Points:

- Seasonal and latitudinal variations of lunar semidiurnal (LSD) tidal magnitudes are revealed via long-term observations by meteor radars
- The quasi-biennial oscillation phases are associated with the enhancement of the LSD during polar vortex weakening events
- A strong quarter-annual oscillation is observed in the LSD magnitudes in the mesosphere and lower thermosphere region

Correspondence to:
Y. Gong,
yun.gong@whu.edu.cn

Citation:
Luo, J., Gong, Y., Ma, Z., Zhang, S., Zhou, Q., Huang, C., et al. (2022). Long-term variation of lunar semidiurnal tides in the MLT region revealed by a meteor radar chain. *Journal of Geophysical Research: Space Physics*, *127*, e2022JA030616. https://doi.org/10.1029/2022JA030616

Received 4 MAY 2022
Accepted 24 AUG 2022

Abstract We present a study on the long-term variation of lunar semidiurnal (LSD) tides in the mesosphere and lower thermosphere (MLT). The study is based on a meteor radar chain along ~120°E meridian, which consists of five stations located at Mohe (MH, 53.5°N, 122.3°E), Beijing (BJ, 40.3°N, 116.2°E), Wuhan (WH, 30.5°N, 114.6°E), Sanya (SY, 18.3°N, 109.6°E), and Ledong (LD, 18.4°N, 109.0°E), respectively. Using the Lomb-Scargle spectral analysis and least squares fitting method, strong quarter-annual oscillations in the LSD are found at the three midlatitude stations and their magnitudes are comparable. The LSD magnitudes exhibit clear seasonal and latitudinal differences. The monthly mean magnitudes of LSD reach the maximum in January at all five stations but in other seasons they behave differently at different stations. Besides, the effects of polar vortex weakening (PVW) and quasi-biennial oscillation (QBO) phases on the LSD are discussed. Based on the 12 PVW events, our study observes that the enhancement of the LSD is not always related to the commencements of PVW events. The enhancements of the LSD during the easterly QBO phase are generally stronger than those enhancements during the westerly QBO phase in the MLT region. The easterly QBO phase could modulate the mesospheric zonal mean zonal winds at low latitudes during the PVWs, which is in favor of amplifying the LSD. Our results suggest that the QBO phase is an important factor in enhancing the LSD in the MLT region during PVW events.

1. Introduction

Atmospheric tides are one of the most important dynamic processes in coupling the lower atmosphere and the upper atmosphere. They are usually observed by radars and satellites in the mesosphere and lower thermosphere (MLT) region. The solar thermal and lunar gravitational tides are the predominant periodic oscillations in the atmosphere. The solar tides, modulated by the variations of water vapor, ozone, and molecular oxygen in the atmosphere, are mainly generated by solar heating (Forbes, 1995). In contrast, the lunar tides are primarily generated by the gravitational forcing of the Moon on the lower atmosphere (Chapman & Lindzen, 1970). Since the forcing is virtually constant, the variations of lunar tides in the MLT region are related to the changes in the background atmosphere (Forbes & Zhang, 2012; Sandford et al., 2007; Yamazaki et al., 2012). Hence, the determination of the lunar tides in the MLT region is an excellent tool to understand the coupling of the atmosphere (Forbes et al., 2013; Stening et al., 1997).

Using numerical simulations, Chapman and Lindzen (1970) predicted that the lunar tides potentially consist of three main modes: Long-term semimonthly lunar tide, lunar diurnal tide, and lunar semidiurnal (LSD) tide. The observed LSD with a period of 12.42 hr consists of a migrating tide with zonal wavenumber 2 (M_2) and a nonmigrating component, which has the largest amplitude among the three modes (Pedatella et al., 2012; Vial & Forbes, 1994). Observations of the LSD in the atmosphere are difficult because the frequency of LSD is very close to the frequency of solar semidiurnal tide. Thus, a high spectral resolution in the data sets is required to distinguish the solar and lunar components.

In the ionosphere, the LSD has been extensively studied using data of the equatorial electrojet (Siddiqui et al., 2015, 2018; Stening, 2011; Yamazaki et al., 2017), the total electron content (Lin et al., 2019; Liu et al., 2019; Pedatella & Forbes, 2010; Sridharan, 2017), the noctilucent clouds (Dalin et al., 2017; Hoffmann et al., 2018;

Table 1
Summary of the Meteor Radar Chain Database

Location	Date/month/year
MH (53.5°N, 122.3°E)	01/08/2011–31/12/2020
BJ (40.3°N, 116.2°E)	04/12/2008–31/12/2020
WH (30.5°N, 114.6°E)	22/09/2010–31/12/2020
SY (18.3°N, 109.6°E)	12/01/2009–16/11/2015
LD (18.4°N, 109.0°E)	16/08/2018–31/12/2020

Fiedler & Baumgarten, 2018; von Savigny et al., 2017), and the temperature and electron density measured from satellites (Forbes & Zhang, 2012, 2019; Forbes et al., 2013; Paulino et al., 2013; Pedatella, 2014; Zhang & Forbes, 2014). In the MLT region, the neutral winds observed by meteor radars and medium-frequency radars provide an advantage to reveal the long-term variations of the LSD. According to the observations from these ground-based radars, the amplitudes and vertical wavelengths of the LSD are investigated from high to low latitudes (Paulino et al., 2015; Sandford et al., 2006, 2007; Sathishkumar et al., 2017; Stening et al., 1987, 1994, 2003). The most important findings of the LSD in the MLT winds can be summarized as (a) the behavior of the LSD amplitudes is very similar in the zonal and meridional winds; (b) the LSD amplitude is most prominent in winter; (c) the LSD has more significant longitudinal variations than the solar semidiurnal tides; and (d) the amplitude of the LSD has a year-to-year variability in both northern and southern hemispheres. However, the latitudinal differences of the LSD in the neutral wind in the MLT region are rarely reported.

Responses of the LSD to the Arctic sudden stratospheric warming (SSW) and polar vortex weakening (PVW) events have been extensively studied in recent years. SSW events mostly occur in the polar region in winter and have significant influences on atmospheric dynamics (e.g., Chau et al., 2012; Gong, Ma, et al., 2018; Gong et al., 2021; Ma et al., 2020). The PVW events can be identified when the stratospheric temperature/zonal mean zonal wind (ZMZW) simultaneously increases/decreases near the polar region during the winter (Zhang & Forbes, 2014). The occurrence of PVW events is almost always accompanied by SSW events (e.g., Albers & Birner, 2014; Ma et al., 2022). Many studies have demonstrated that the LSD amplitude is enhanced during SSW/PVW events (Forbes & Zhang, 2012; Li et al., 2021; Siddiqui et al., 2015, 2018; Wu et al., 2019). Zhang and Forbes (2014) suggested that the enhancement of the LSD at 110 km occurs just after the commencement of PVWs and the LSD amplitude increases with the enhancement of PVWs. Chau et al. (2015) found that the time and magnitude of the LSD are highly related to the onset dates and magnitudes of PVWs. He and Chau (2019) proposed that the strongest enhancement of M_2 occurs in vortex-split PVW/SSW events. Koushik et al. (2020) suggested that the occurrence of the LSD enhancement is closer to the onset date of PVWs rather than SSWs.

In the present study, we use the wind observations obtained from a meteor radar chain to investigate the LSD activities from the middle to low latitudes in the northern hemisphere. Our primary goal is to study climatology and latitudinal variation of the LSD from middle to low latitudes and investigate the association between the LSD and PVW events from 2009 to 2020 in the MLT region. The paper is organized as follows. In Section 2, we introduce the data and methods to extract the amplitudes of the LSD. Section 3 presents the long-term variations of the LSD. Discussions are given in Section 4. Conclusions are summarized in Section 5.

2. Data Analysis

In this study, horizontal winds in the MLT region are obtained from five meteor radars located along ~120°E meridian in the northern hemisphere, which consists of five stations located at Mohe (MH, 53.5°N, 122.3°E), Beijing (BJ, 40.3°N, 116.2°E), Wuhan (WH, 30.5°N, 114.6°E), Sanya (SY, 18.3°N, 109.6°E), and Ledong (LD, 18.4°N, 109.0°E), respectively. These all-sky meteor radars use the interferometry technique to detect the meteor echoes and retrieve the drift speeds of meteor trails, which are used to calculate the neutral winds via the least squares fitting method within a spatial and temporal window (Hocking et al., 2001). The meridional winds (positive northward) and the zonal winds (positive eastward) have a 1-hr temporal resolution and a 2-km vertical resolution from 80 to 96 km. The observational calendars of each meteor radar are presented in Table 1. Note that the meteor radar at SY was not in use in 2015 and a new meteor radar was established in a neighboring site of LD in 2018. The observations of SY and LD are analyzed together as the SY-LD site in the present study. Please refer to previous studies for detailed information on the meteor radars and MLT wind products (e.g., Li et al., 2012; Ma et al., 2018; Yu et al., 2013).

The least squares fitting method is used to extract the amplitudes of the LSD from the hourly meridional and zonal winds, which can be expressed as follows:

$$a(t) = A_0 + A_1 \cos\left(\frac{2\pi t}{24} - \varphi_1\right) + A_2 \cos\left(\frac{2\pi t}{12} - \varphi_2\right) + A_3 \cos\left(\frac{2\pi t}{12.42} - \varphi_3\right) \quad (1)$$

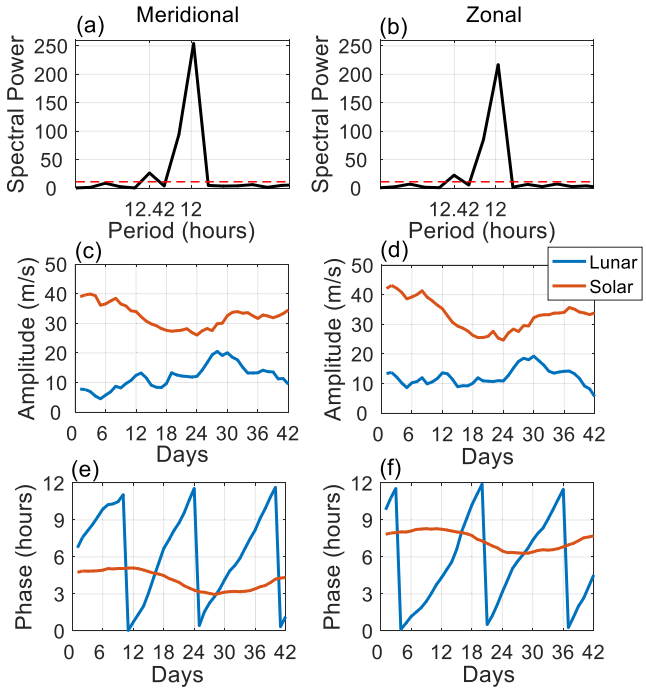

Figure 1. (a–b) The Lomb-Scargle spectral in the meridional and zonal winds at 96 km over MH from 1 December, 2014 to 31 January, 2015. The red dashed lines present the 95% confidence level of spectral. (c–d) The amplitudes of lunar semidiurnal (LSD) tides and solar semidiurnal tides in the meridional and zonal winds. (e–f) The phases of LSD and solar semidiurnal tides in the meridional and zonal winds.

where t is the time in hours in the solar time frame; A_0 is the mean background wind; and A_i and φ_i are the amplitudes and phases of solar diurnal, solar semidiurnal, and LSD tide. In order to distinguish the solar and LSD tides, the length of the fitting window (N, number of days) should satisfy the condition $\frac{1}{N*24} < \frac{1}{12} - \frac{1}{12.42}$, which means N > 14.79. In this study, a 21-day sliding window shifted by 1 day is used (e.g., Chau et al., 2015; Conte et al., 2017, 2019). In each sliding window, the fitting is only performed when the missing data are less than 100 hr (20% of the 21 days).

Figure 1 presents the results of the Lomb-Scargle spectral analysis (a, b) and the amplitude (c, d) and phase (e, f) of the LSD (blue) and solar (red) semidiurnal tide using the meridional (left) and zonal (right) winds at 96 km over MH from 1 December, 2014 to 31 January, 2015. In Figures 1a and 1b, two peaks at around 12 and 12.42 hr can be clearly seen from the spectra in both meridional and zonal components. Both peaks are above the 95% confidence level that is indicated by the dashed red lines. As shown in Figures 1c and 1d, the daily variations of the LSD amplitudes are very different from solar semidiurnal tides. The correlation between the amplitudes of LSD and solar semidiurnal tides are −0.32 and −0.03 in the meridional and zonal components, respectively. The results indicate that the LSD and solar semidiurnal tides have limited mutual dependence. As seen from Figures 1e and 1f, the variation of LSD phases has a period of about 14 days, which is a typical characteristic of LSD phases in the solar time frame (Lin et al., 2019). The LSD phases have a solar time shift, which is due to the time difference between the Sun and the Moon crossing the same longitude on Earth. The phases of solar semidiurnal tides vary within a period of 3 hr, which is very different from the phase behavior of the LSD. The results shown in Figure 1 demonstrate that the LSD and solar semidiurnal tides can be successfully separated using the methods described above.

The Modern-Era Retrospective Analysis for Research and Applications-2 (MERRA2) reanalysis data are used to reveal the variations of the middle atmosphere. The reanalysis data have a geographical resolution of 0.5° × 0.625° and a temporal resolution of 1 day. The ZMZW and temperature are used to identify the onset dates of PVW events. A detailed description of the MERRA2 reanalysis data can be found in Gelaro et al. (2017).

The Singapore-based radiosonde monthly mean zonal winds are downloaded from the Free University of Berlin repository, which is used to reveal the quasi-biennial oscillation (QBO) phases (e.g., Laskar et al., 2016; Sathishkumar et al., 2017).

3. Results

The LSD amplitudes are, respectively, extracted in the zonal and meridional components (A_u and A_v). Following previous studies (e.g., Chau et al., 2015; Conte et al., 2017, 2019), the total magnitude ($\sqrt{A_u{}^2 + A_v{}^2}$) is calculated and regarded as the magnitude of the LSD. Figure 2 presents the daily magnitudes of the LSD at MH (53°N), BJ (40°N), WH (30°N), and SY-LD (18°N) from 1 January 2009 to 20 December 2020. Note that the date of the amplitude is labeled as the central date of the 21-day fitting window. As shown in Figure 2, the maximum magnitudes of the LSD reach up to 27.9 m/s on 9 January 2015 at MH, 36.2 m/s on 11 January 2015 at BJ, 27.0 m/s on 28 January 2013 at WH, and 25.9 m/s on 6 January 2020 at LD, respectively. It appears that the LSD in the MLT region has clear interannual and intra-annual variations.

The annual oscillation (AO), semiannual oscillation (SAO), ter-annual oscillation (TAO), and quarter-annual oscillation (QAO) are usually observed in the MLT region (e.g., Day et al., 2012; Ma et al., 2018). Using the same meteor radar chain, Ma et al. (2018) reported that the AO dominates the neutral winds at middle latitudes while both the AO and SAO are important at low latitudes. The interannual and intra-AOs are also widely observed in solar tides and planetary waves in the MLT region (e.g., Gong, Li, et al., 2018; Lu et al., 2011). However, the interannual and intra-AOs in the LSD magnitudes have been rarely reported in previous studies. The present study

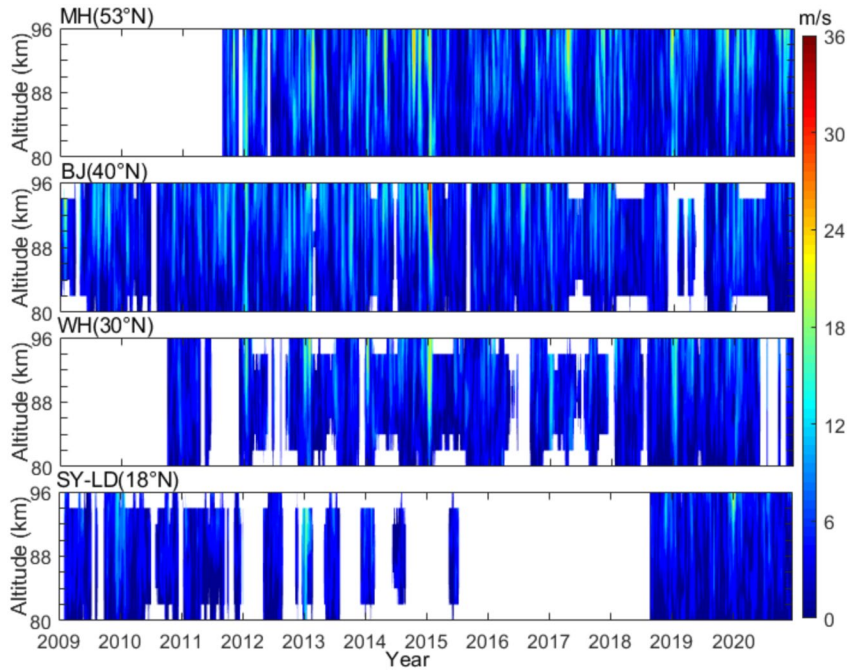

Figure 2. The daily variation of the magnitude of lunar semidiurnal tides at MH, BJ, WH, and LD-SY (from top to bottom) from 1 January 2009 to 20 December 2020.

investigates the interannual and intra-AOs in the LSD based on about 10 years of observations. The investigation is made by a Lomb-Scargle spectral analysis and the results are shown in Figure 3. Note that the results at SY-LD are not shown due to a large amount of missing data from 2015 to 2018. In Figure 3, spectral values under the 95% confidence level are set to zero. As shown in the left column of Figure 3, the AO, QAO, and SAO are the most prominent oscillations in the amplitudes of the LSD at MH, BJ, and WH, respectively.

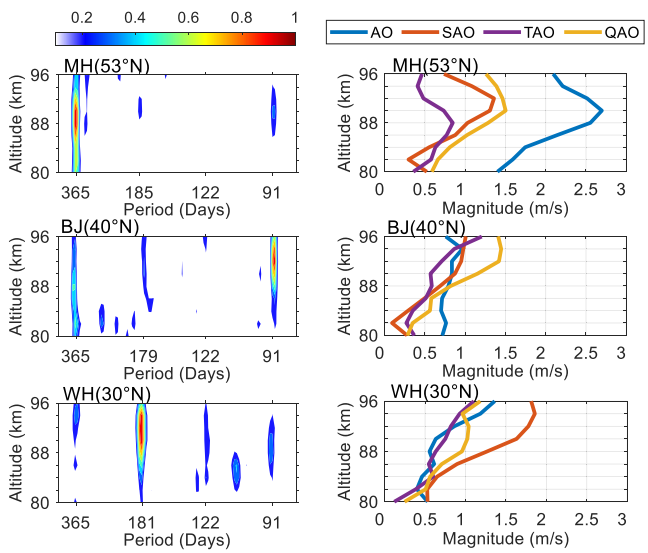

Figure 3. The left column is the Lomb-Scargle periodogram of daily lunar semidiurnal magnitudes at MH, BJ, and WH, respectively. The right column is the magnitude of annual oscillation, semiannual oscillation, ter-annual oscillation, and quarter-annual oscillation, respectively.

The amplitudes of AO, SAO, TAO, and QAO are extracted from the daily magnitudes of the LSD at each altitude using the least squares fitting method via the following equation:

$$A(d) = B_0 + B_1 \cos\left(\frac{2\pi d}{T_{\mathrm{AO}}} - \phi_1\right) + B_2 \cos\left(\frac{2\pi d}{T_{\mathrm{SAO}}} - \phi_2\right) + B_3 \cos\left(\frac{2\pi d}{T_{\mathrm{TAO}}} - \phi_3\right) + B_4 \cos\left(\frac{2\pi d}{T_{\mathrm{QAO}}} - \phi_4\right) \quad (2)$$

where d is time in days; B_0 is the background level; and B_{i} and ϕ_i are the amplitudes and phases of each oscillation. The T_{AO}, T_{SAO}, T_{TAO}, and T_{QAO} are, respectively, the periods of AO, SAO, TAO, and QAO, which are derived based on the left column of Figure 3. In this study, the T_{AO}, T_{TAO}, and T_{QAO} are 365 days, 122 days, and 91 days at the three stations, respectively. The T_{SAO} is 185 days at MH, 179 days at BJ, and 181 days at WH. The fitted results are shown in the right column of Figure 3. The amplitude of AO at MH is the strongest oscillation among all stations, which is about twice the AO amplitudes at BJ and WH. In general, the TAO is the weakest oscillation at all three stations. The SAO is the strongest component at WH but relatively weak at MH and BJ. Interestingly, the QAO is strong at all three stations and its amplitude is comparable at the three stations, which indicates that the QAO is important in the long-term variability of the LSD magnitudes.

To illustrate the seasonal variations of the LSD, monthly mean magnitudes are averaged from the daily magnitudes and are further computed into a composite year. The monthly mean results are only performed when the daily

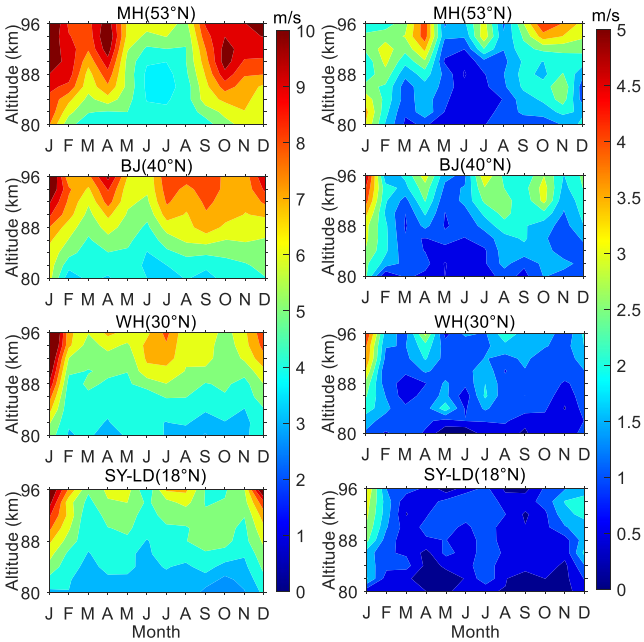

Figure 4. Monthly mean magnitudes of the lunar semidiurnal (left column) and standard deviations (right column) in a composite year at MH, BJ, WH, and SY-LD (from top to bottom), respectively. Contour steps are 1 m/s.

magnitudes are available more than 20 days in each month. Figure 4 presents the monthly mean magnitudes of the LSD and the standard deviations in a composite year at MH, BJ, WH, and SY-LD. As shown in the left column of Figure 4, the LSD magnitudes roughly increase with increasing altitude in the MLT region at all four sites. The LSD magnitudes at MH are enhanced with three peaks in December-January, April, and October. At BJ, four peaks appear in December-January, April, July, and September. The magnitudes of the LSD at WH are enhanced in December-January and July. In the site of SY-LD, the strongest enhancement is observed in December-January, while two moderate enhancements appear in April-May and July-August. As shown in the right column of Figure 4, the standard deviations are relatively great in April and October at MH, in January, April, July, and October at BJ, in January and April at WH, and in January at SY-LD, which means that the year-to-year variability of LSD is obvious in these months. Figures 3 and 4 have clear consistencies that the AO, QAO, and SAO are, respectively, the strongest oscillations at MH, BJ, and WH, which can be well observed in both figures. Note that the discrepancy between Figures 3 and 4 is mainly due to the large year-to-year variability of the LSD.

The seasonal variations shown in Figure 4 are generally consistent with previous studies (e.g., Conte et al., 2017; He & Chau, 2019) but with one discrepancy. Our results indicate that the LSD is enhanced in April at MH, while observations from the meteor radars at similar latitudes at Castle Eaton (52.6°N, 2.19°W) and Juliusruh (54.6°N, 13.4°E) indicate weak magnitudes in April (e.g., Conte et al., 2017; Sandford et al., 2006). The discrepancy is very likely due to the longitudinal distribution of LSD, which is caused by the nonmigrating lunar tides (Forbes & Zhang, 2019).

Clear latitudinal differences can be seen in Figure 4. At MH and BJ, an enhancement of the LSD magnitude occurs in April, while it does not appear at WH and SY-LD. At MH, the magnitude is weak around July below 94 km, while it is strong above 86 km at BJ and WH. At SY-LD, the magnitude is weak below 88 km throughout the year. At BJ, the magnitude is continuously larger than 5 m/s above 86 km throughout the year. Based on the observations from three meteor radars located in the Brazilian sector, Paulino et al. (2015) suggested that the latitudinal variations of the LSD are caused by different dominant Hough modes of the LSD in different months.

Table 2
The Onset Dates of Polar Vortex Weakening (PVW) Events From 2009 to 2020

Year	Onset date of PVW (month/day)
2009	01/23
2010	01/29
2011	01/31
2012	01/17
2013	01/11
2014	02/08
2015	01/05
2016	02/09
2017	01/30
2018	02/14
2018	12/31
2020	02/05

4. Discussions

Previous studies suggested that the enhancements of the LSD in the MLT region are associated with the Arctic PVW events, which are accompanied by the attenuations or reversals of the easterly ZMZW in the middle atmosphere (e.g., Chau et al., 2015; Conte et al., 2017; He & Chau, 2019; Koushik et al., 2020; Zhang & Forbes, 2014). The attenuations of ZMZW in the middle atmosphere are thought to contribute to the amplifications of the LSD magnitudes (Forbes & Zhang, 2012). In this study, we further examine the effect of PVWs on the LSD based on the long-term meteor wind observations from 2009 to 2020, which extends the statistical analyses of PVW events only before the year 2013 in previous studies.

Zhang and Forbes (2014) first identified the PVW by the daily time series of two parameters: The temperature at 90°N and 40 km and the ZMZW at 70°N and 48 km. The onset date of a PVW event is defined when the first local maximum of the temperature and the minimum of the ZMZW are simultaneously observed in the first 60 days of a year. If the local maximum temperature and the minimum ZMZW are not simultaneously captured, the onset date is only defined at the date when the minimum ZMZW occurs (e.g., Zhang & Forbes, 2014). Following these definitions, the onset dates

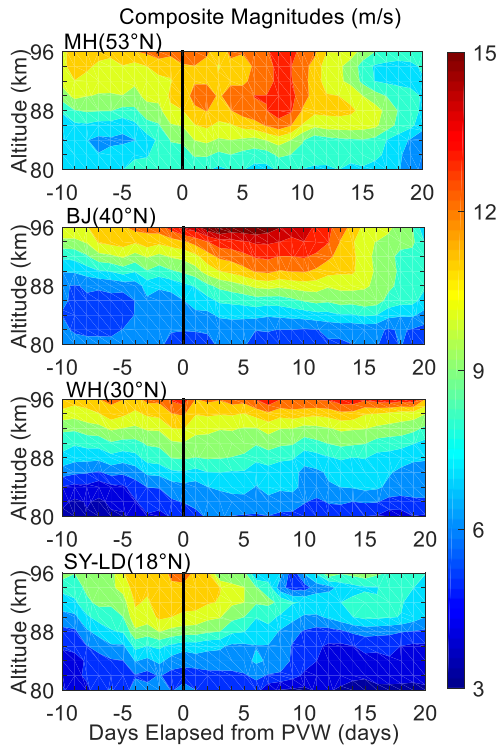

Figure 5. Composite lunar semidiurnal magnitudes from 10 days before to 20 days after the onset dates of polar vortex weakenings (PVWs) at MH, BJ, WH, and SY-LD (from top to bottom), respectively. Black lines present the onset dates of PVWs. Contour steps are 1 m/s.

of PVW events from 2009 to 2020 are found and listed in Table 2. Based on the onset dates of PVW shown in Table 2, the composite LSD magnitudes over MH, BJ, WH, and SY-LD from 10 days before to 20 days after the onset dates are calculated in Figure 5. As shown in Figure 5, the LSD magnitudes generally increase after the onset date of PVW at MH and BJ. The strongest response of the LSD to PVW is observed at BJ, with a maximum magnitude over 15 m/s at 96 km. However, the LSD at WH does not reveal obvious changes before and after the commencement of PVW. The LSD at SY-LD is enhanced earlier with the occurrence of PVW but decreases in a week after the PVW. Results shown in Figure 5 suggest that the enhancements of the LSD are not always related to the commencement of PVW events. Our result indicates that the enhancements of the LSD cannot be fully explained by the modulation of PVW events at WH and SY-LD (lower latitudes).

The QBO in the equatorial stratospheric zonal wind can significantly modulate the solar tides and neutral winds in the MLT region (e.g., Forbes et al., 2008; Laskar et al., 2016; Wu et al., 2008). Based on two meteor radars located at high and middle latitudes, Laskar et al. (2016) reported that the amplitudes of solar semidiurnal tides are above the mean level when the QBO phase is eastward. In the following, we intend to investigate the effects of the QBO phase on the LSD during PVW events. The QBO phases are determined by the directions of the monthly mean zonal winds at the equator (named QBO-related winds), which can be derived from radiosonde near the equator (Naujokat, 1986) and have been widely accepted. The positive QBO-related wind presents the westerly QBO phase, while the negative QBO-related wind presents the easterly QBO phase. Figure 6 presents (a) the QBO-related monthly mean zonal winds from January 2009 to December 2020 and (b) the evolutions of QBO winds averaged from 50 hPa to 30 hPa. In Figure 6a, the white lines represent zero wind lines. As shown in Figure 6a, the QBO-related monthly mean zonal winds at the equator reveal clear alternating westerly QBO phases and easterly QBO phases from 2009 to 2020. The zonal winds averaged from 50 hPa to 30 hPa presented in Figure 6b are used to identify the QBO phases (e.g., Laskar et al., 2016; Sathishkumar et al., 2017). The dots of the averaged QBO-related winds in the months when the PVWs happened are highlighted. The blue and red dots in Figure 6b represent the westerly and easterly QBO phases (QBOw and QBOe) with the occurrence of PVW, respectively. This definition

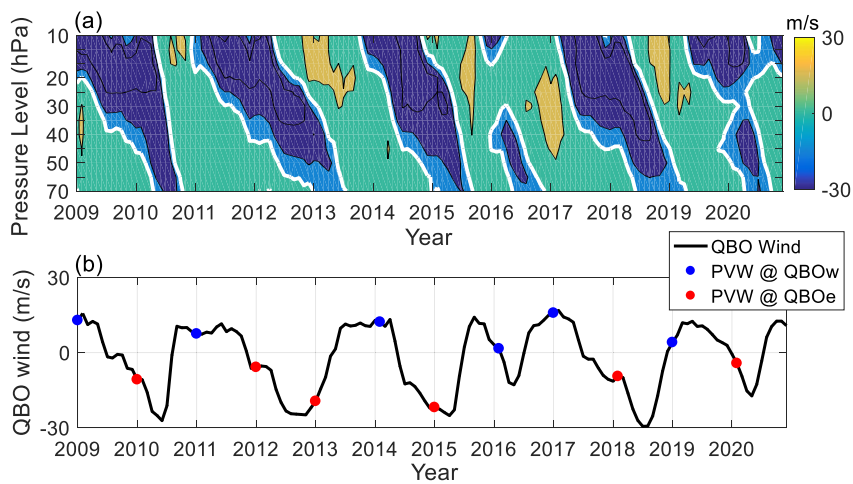

Figure 6. (a) The quasi-biennial oscillation (QBO)-related monthly mean zonal winds from January 2009 to December 2020. The white lines represent zero wind lines. (b) The QBO-related winds averaged from 30 hPa to 50 hPa. The westerly and easterly QBO phases (QBOw and QBOe) with the occurrence of polar vortex weakening are, respectively, presented by the blue and red dots.

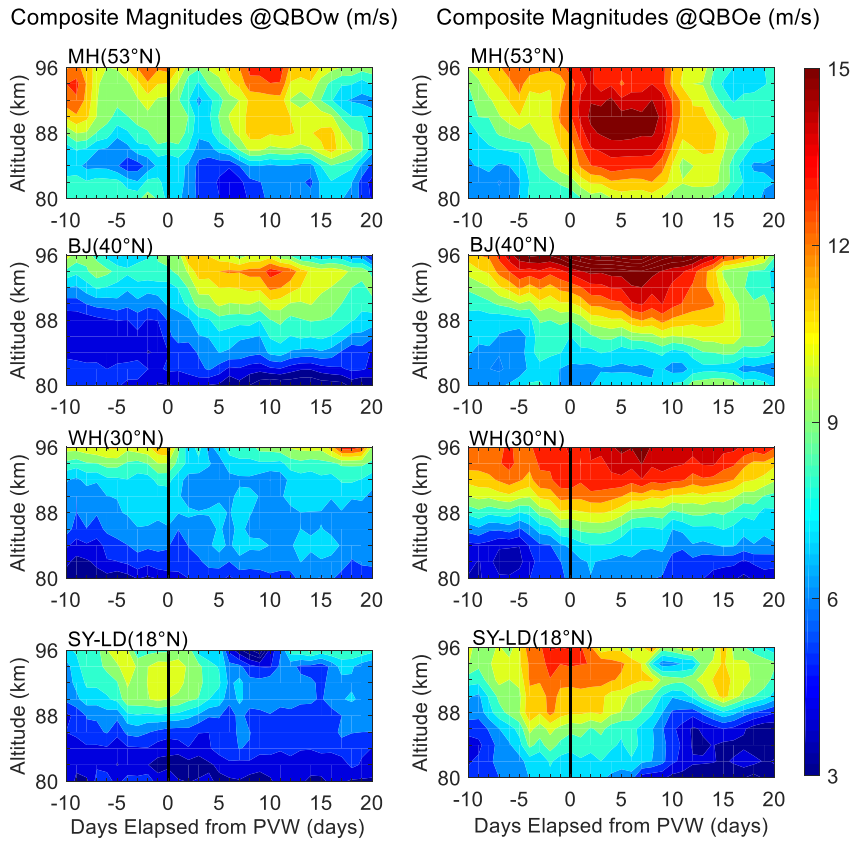

Figure 7. Same as Figure 5 but during the QBOw (left column) and the QBOe (right column).

is selected because the QBO-related winds from 50 hPa to 30 hPa are well correlated with the variabilities of the Arctic polar vortex in the winter (Anstey & Sheperd, 2014; Garfinkel et al., 2012). In the 12 years of observation, six PVW events occur in the QBOw (blue dots) and six PVW events are observed during the QBOe (red dots).

According to the different phases of QBOs, the composite LSD amplitudes are recalculated from 10 days before to 20 days after the onset dates of PVWs during QBOw and QBOe, respectively. As shown in Figure 7, the LSD magnitudes during QBOe (right column of Figure 7) are generally stronger than those enhancements during QBOw (left column of Figure 7) at all four latitudes. Particularly, the magnitudes of the LSD at WH even decrease around five days after the onset of PVW during QBOw. This may be the reason that the evolution of the LSD at WH has no clear relation with the commencement of PVWs, which is illustrated in Figure 5. Our results suggest that the QBO phases may play an important role in the enhancement of the LSD in the northern hemispheric MLT region.

Since the weakening of the ZMZW is important in amplifying the LSD during PVW events (Forbes & Zhang, 2012), the association between the ZMZW and the QBO phases during PVWs is investigated. Using the MERRA2 reanalysis data, the ZMZW from 60 to 80 km at the latitude of each station are obtained on days −3, 0, 3, 6, and 9 (zero represents the onset of the PVW). We perform a comparison of the composite ZMZW during PVW events between the QBOw (blue) and QBOe (red) and the results are shown in Figure 8. As seen from Figure 8, the composite ZMZW during QBOe is weaker than ZMZW during QBOw from day −3 to day 9 at low latitudes (WH and SY-LD stations) and from day −3 to day 3 at BJ latitude. At the highest latitude station MH, the ZMZW during QBOe is much weaker than the ZMZW during QBOw on day 0. These results suggest that the QBOe could reduce the ZMZW in the mesosphere at low latitudes during the PVW events. Our study indicates that attenuations of the mesospheric ZMZW during the QBOe periods could be in favor of amplifying the LSD magnitudes at low latitudes.

The QBO phases can affect the propagating and breaking of stationary planetary waves, which break more heavily in the polar region and cause a more disturbed polar vortex during QBOe than QBOw (Holton & Austin, 1991;

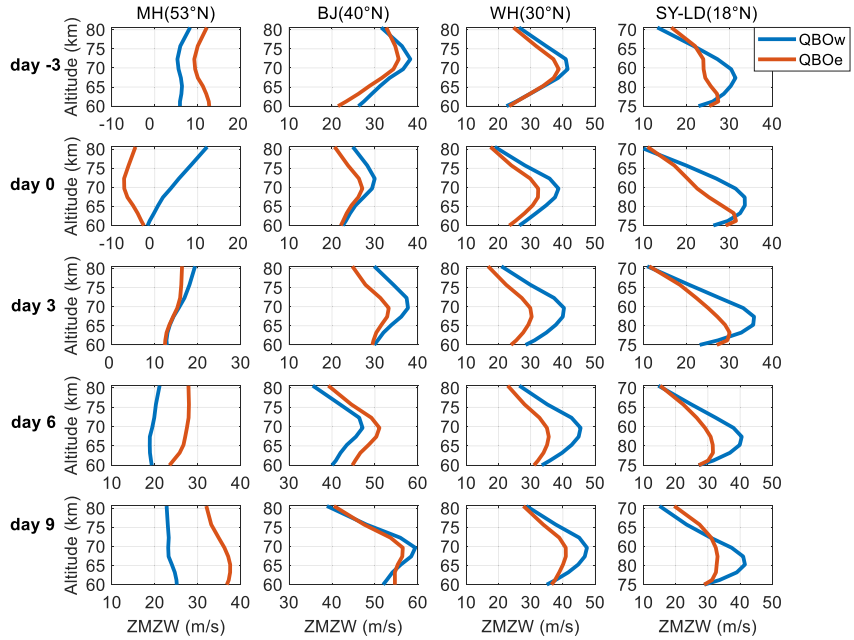

Figure 8. The composite mesospheric zonal mean zonal wind on the days −3, 0, 3, 6, and 9 (zero represents the onset of the polar vortex weakening) during QBOw (blue) and QBOe (red) at the latitudes of MH, BJ, WH, and SY-LD stations.

Siddiqui et al., 2018). The ZMZWs are attenuated when the polar vortex weakens. Then, the weaker ZMZW during QBOe might lead to the enhancements of LSD at low latitudes. However, at the highest latitude station MH, the time of attenuated mesospheric ZMZW does not correspond well with the enhancements of LSD. The nonlinear interactions between the 16 days planetary waves and solar semidiurnal tides might also contribute to the amplification of LSD (He & Chau, 2019). Nevertheless, further studies on the influences of attenuated ZMZW during QBOe on the LSD at high latitudes are needed.

5. Summary and Conclusions

Based on long-term neutral wind measurements by meteor radars located at Mohe (MH, 53.5°N, 122.3°E), Beijing (BJ, 40.3°N, 116.2°E), Wuhan (WH, 30.5°N, 114.6°E), Sanya (SY, 18.3°N, 109.6°E), and Ledong (LD, 18.4°N, 109.0°E) from 2009 to 2020, the amplitudes of the LSD tides in the MLT region are extracted using the least squares fitting method. The total magnitudes of the LSD are calculated based on the LSD amplitudes in both zonal and meridional components. Using the obtained LSD magnitudes and the MERRA2 reanalysis and Singapore-based radiosonde data from 2009 to 2020, we present analyses of the interannual and intra-AOs in the LSD magnitudes, the seasonal and latitudinal variations of the LSD magnitudes, and the effects of PVW events and QBO phases on the enhancements of the LSD. Major findings are as follows:

The AO, QAO, and SAO in the LSD magnitudes, respectively, dominate at MH, BJ, and WH. The AO amplitude at MH is about twice the AO amplitudes at BJ and WH. The QAO is relatively strong and its magnitude is comparable at the three stations, which indicates that the QAO in the LSD magnitudes is important in the MLT region at midlatitudes. The seasonal variations of the LSD show clear latitudinal differences from middle to low latitudes. The monthly mean magnitudes of the LSD reach the maximum in January at all four latitudes, while in other seasons, the LSD magnitudes behave differently at the different latitudes.

Based on our investigation on 12 PVW events from 2009 to 2020, the enhancements of the LSD are not always related to the commencement of PVWs. We found that the enhancements of the LSD during the easterly QBO phases (QBOe) periods are generally stronger than those enhancements during the westerly QBO phases (QBOw) periods. The mesospheric ZMZWs at low latitudes during the PVWs, modulated by the QBO phases, are found to be weaker during the QBOe than those during the QBOw, which can lead to the stronger enhancements of the LSD at low latitudes during PVWs. Our results indicate that the QBO phases play an important role in influencing the LSD magnitude in the MLT region during PVW events.

Data Availability Statement

The meteor radars data are provided by BNOSE, IGGCAS through the Data Center for Geophysics, and National Earth System Science Data Sharing Infrastructure (http://wdc.geophys.ac.cn/index.asp). The Singapore-based radiosonde monthly mean zonal winds are downloaded from the Free University of Berlin repository (https://www.geo.fu-berlin.de/en/met/ag/strat/produkte/qbo/). The Modern-Era Retrospective Analysis for Research and Applications-2 reanalysis data is available on the website of https://disc.gsfc.nasa.gov/datasets.

Acknowledgments
The Project was supported by the Open Fund of Hubei Luojia Laboratory, the National Natural Science Foundation of China (through grants 41574142, 42104145, and 42127805), the China Postdoctoral Science Foundation (through grants 2021M692465 and 2020TQ0230), and the U.S. National Science Foundation grant AGS-2152109. We acknowledge the use of radar data from the Chinese Meridian Project.

References

Albers, J. R., & Birner, T. (2014). Vortex preconditioning due to planetary and gravity waves prior to sudden stratospheric warmings. *Journal of the Atmospheric Sciences*, *71*(11), 4028–4054. https://doi.org/10.1175/JAS-D-14-0026.1

Anstey, J. A., & Sheperd, T. G. (2014). High-latitude influence of the quasi-biennial oscillation. *Quarterly Journal of the Royal Meteorological Society*, *140*(678), 1–21. https://doi.org/10.1002/qj.2132

Chapman, S., & Lindzen, R. S. (1970). *Atmospheric tides: Thermal and gravitational* (p. 200). Gordon and Breach.

Chau, J. L., Goncharenko, L. P., Fejer, B. G., & Liu, H. L. (2012). Equatorial and low latitude ionospheric effects during sudden stratospheric warming events. *Space Science Reviews*, *168*(1–4), 385–417. https://doi.org/10.1007/s11214-011-9797-5

Chau, J. L., Hoffmann, P., Pedatella, N. M., Matthias, V., & Stober, G. (2015). Upper mesospheric lunar tides over middle and high latitudes during sudden stratospheric warming events. *Journal of Geophysical Research: Space Physics*, *120*(4), 3084–3096. https://doi.org/10.1002/2015JA020998

Conte, J. F., Chau, J. L., & Peters, D. H. W. (2019). Middle- and high-latitude mesosphere and lower thermosphere mean winds and tides in response to strong polar-night jet oscillations. *Journal of Geophysical Research: Atmosphere*, *124*(16), 9262–9276. https://doi.org/10.1029/2019JD030828

Conte, J. F., Chau, J. L., Stober, G., Pedatella, N., Maute, A., Hoffmann, P., et al. (2017). Climatology of semidiurnal lunar and solar tides at middle and high latitudes: Interhemispheric comparison. *Journal of Geophysical Research: Space Physics*, *122*(7), 7750–7760. https://doi.org/10.1002/2017JA024396

Dalin, P., Kirkwood, S., Pertsev, N., & Perminov, V. (2017). Influence of solar and lunar tides on the mesopause region as observed in polar mesosphere summer echoes characteristics. *Journal of Geophysical Research: Atmosphere*, *122*(19), 10369–10383. https://doi.org/10.1002/2017JD026509

Day, K., Taylor, M., & Mitchell, N. (2012). Mean winds, temperatures and the 16- and 5-day planetary waves in the mesosphere and lower thermosphere over bear Lake observatory (42°N, 111°W). *Atmospheric Chemistry and Physics*, *12*(3), 1571–1585. https://doi.org/10.5194/acp-12-1571-2012

Fiedler, J., & Baumgarten, G. (2018). Solar and lunar tides in noctilucent clouds as determined by ground-based lidar. *Atmospheric Chemistry and Physics*, *18*(21), 16051–16061. https://doi.org/10.5194/acp-18-16051-2018

Forbes, J. M. (1995). Tidal and planetary waves (a tutorial). In R. M. Johnson & T. L. Killeen (Eds.), *The upper mesosphere and lower thermosphere: A review of experiment and theory*, *Geophysical monograph series* (Vol. 87, p. 356). AGU.

Forbes, J. M., & Zhang, X. (2012). Lunar tide amplification during the January 2009 stratosphere warming event: Observations and theory. *Journal of Geophysical Research*, *117*(A12), A12312. https://doi.org/10.1029/2012JA017963

Forbes, J. M., & Zhang, X. (2019). Lunar tide in the F region ionosphere. *Journal of Geophysical Research: Space Physics*, *124*(9), 7654–7669. https://doi.org/10.1029/2019JA026603

Forbes, J. M., Zhang, X., Bruinsma, S., & Oberheide, J. (2013). Lunar semidiurnal tide in the thermosphere under solar minimum conditions. *Journal of Geophysical Research: Space Physics*, *118*(4), 1788–1801. https://doi.org/10.1029/2012JA017962

Forbes, J. M., Zhang, X., Palo, S., Russell, J., Mertens, C. J., & Mlynczak, M. (2008). Tidal variability in the ionospheric dynamo region. *Journal of Geophysical Research*, *113*(A2), A02310. https://doi.org/10.1029/2007JA012737

Garfinkel, C. I., Shaw, T. A., Hartmann, D. L., & Waugh, D. W. (2012). Does the holton-tan mechanism explain how the quasi-biennial oscillation modulates the Arctic polar vortex? *Journal of the Atmospheric Sciences*, *69*(5), 1713–1733. https://doi.org/10.1175/JAS-D-11-0209.1

Gelaro, R., McCarty, W., Suarez, M. J., Todling, R., Molod, A., Takacs, L., et al. (2017). The modern-era retrospective analysis for research and applications, Version 2 (MERRA-2). *Journal of Climate*, *30*(14), 5419–5454. https://doi.org/10.1175/JCLI-D-16-0758.1

Gong, Y., Li, C., Ma, Z., Zhang, S., Zhou, Q., Huang, C., et al. (2018a). Study of the quasi-5-day wave in the MLT region by a meteor radar chain. *Journal of Geophysical Research: Atmosphere*, *123*(17), 9474–9487. https://doi.org/10.1029/2018JD029355

Gong, Y., Ma, Z., Lv, X., Zhang, S., Zhou, Q., Aponte, N., & Sulzer, M. (2018b). A study on the quarterdiurnal tide in the thermosphere at Arecibo during the February 2016 sudden stratospheric warming event. *Geophysical Research Letters*, *45*(23), 13142–13149. https://doi.org/10.1029/2018GL080422

Gong, Y., Xue, J., Ma, Z., Zhang, S., Zhou, Q., Huang, C., et al. (2021). Strong quarterdiurnal tides in the mesosphere and lower thermosphere during the 2019 Arctic sudden stratospheric warming over Mohe, China. *Journal of Geophysical Research: Space Physics*, *126*(10), e2020JA029066. https://doi.org/10.1029/2020JA029066

He, M., & Chau, J. L. (2019). Mesospheric semidiurnal tides and near-12 h waves through jointly analyzing observations of five specular meteor radars from three longitudinal sectors at boreal midlatitudes. *Atmospheric Chemistry and Physics*, *19*(9), 5993–6006. https://doi.org/10.5194/acp-19-5993-2019

Hocking, W., Fuller, B., & Vandepeer, B. (2001). Rea-time determination of meteor-related parameters utilizing modern digital technology. *Journal of Atmospheric and Solar-Terrestrial Physics*, *63*(2–3), 155–169. https://doi.org/10.1016/s1364-6826(00)00138-3

Hoffmann, C. G., von Savigny, C., Hervig, M. E., & Oberbremer, E. (2018). The lunar semidiurnal tide at the polar summer mesopause observed by SOFIE. *Journal of Atmospheric and Solar-Terrestrial Physics*, *167*, 134–145. https://doi.org/10.1016/j.jastp.2017.11.014

Holton, J. R., & Austin, J. (1991). The influence of the equatorial QBO on sudden stratospheric warmings. *Journal of the Atmospheric Sciences*, *48*(4), 607–618. https://doi.org/10.1175/1520-0469(1991)048<0607:TIOTEQ>2.0.CO;2

Koushik, N., Kumar, K. K., Vineeth, C., Ramkumar, G., & Subrahmanyam, K. V. (2020). Meteor radar observations of lunar semidiurnal oscillations in the mesosphere lower thermosphere over low and equatorial latitudes and their variability during sudden stratospheric warming events. *Journal of Geophysical Research: Space Physics*, *125*(9), e2019JA027736. https://doi.org/10.1029/2019JA027736

Laskar, F. I., Chau, J. L., Stober, G., Hoffmann, P., Hall, C. M., & Tsutsumi, M. (2016). Quasi-biennial oscillation modulation of the middle and high-latitude mesospheric semidiurnal tides during August-September. *Journal of Geophysical Research: Space Physics*, *121*(5), 4869–4879. https://doi.org/10.1002/2015JA022065

Li, G., Ning, B., Hu, L., Chu, Y.-H., Reid, I. M., & Dolman, B. K. (2012). A comparison of lower thermospheric winds derived from range spread and specular meteor trail echoes. *Journal of Geophysical Research*, *117*(A3), A03310. https://doi.org/10.1029/2011JA016847

Li, Y., Chen, G., Zhang, S., Gong, W., Ma, Z., Huang, K., & Gong, Y. (2021). Effect of semidiurnal lunar tides modulated by quasi-2-day wave on equatorial electrojet during three sudden stratospheric warming events. *Geophysical Research Letters*, *48*(19), e2021GL095352. https://doi.org/10.1029/2021GL095352

Lin, J. T., Lin, C. H., Lin, C. Y., Pedatella, N. M., Rajesh, P. K., Matsuo, T., & Liu, J. Y. (2019). Revisiting the modulations of ionospheric solar and lunar migrating tides during the 2009 stratospheric sudden warming by using global ionosphere specification. *Space Weather*, *17*(5), 767–777. https://doi.org/10.1029/2019SW002184

Liu, J., Zhang, D.-H., Hao, Y.-Q., & Xiao, Z. (2019). The comparison of lunar tidal characteristics in the low-latitudinal ionosphere between East Asian and American sectors during stratospheric sudden warming events: 2009–2018. *Journal of Geophysical Research: Space Physics*, *124*(8), 7013–7033. https://doi.org/10.1029/2019JA026722

Lu, X., Liu, A. Z., Oberheide, J., Wu, Q., Li, T., Li, Z., et al. (2011). Seasonal variability of the diurnal tide in the mesosphere and lower thermosphere over Maui, Hawaii (20.7°N, 156.3°W). *Journal of Geophysical Research*, *116*(D17), D17103. https://doi.org/10.1029/2011JD015599

Ma, Z., Gong, Y., Zhang, S., Zhou, Q., Huang, C., Huang, K., et al. (2018). Study of mean wind variations and gravity wave forcing via a meteor radar chain and comparison with HWM-07 results. *Journal of Geophysical Research: Atmosphere*, *123*(17), 9488–9501. https://doi.org/10.1029/2018JD028799

Ma, Z., Gong, Y., Zhang, S., Zhou, Q., Huang, C., Huang, K., & Li, G. (2022). First observational evidence for the role of polar vortex strength in modulating the activity of planetary waves in the MLT region. *Geophysical Research Letters*, *49*(3), e2021GL096548. https://doi.org/10.1029/2021GL096548

Ma, Z., Gong, Y., Zhang, S. D., Luo, J. H., Zhou, Q. H., Huang, C. M., et al. (2020). Comparison of stratospheric evolution during the major sudden stratospheric warming events in 2018 and 2019. *Earth and Planetary Physics*, *4*(5), 493–503. https://doi.org/10.26464/epp2020044

Naujokat, B. (1986). An update of the observed quasi-biennial oscillation of the stratospheric winds over the tropics. *Journal of the Atmospheric Sciences*, *43*(17), 1873–1877. https://doi.org/10.1175/1520-0469(1986)043<1873:AUOTOQ>2.0.CO;2

Paulino, A. R., Batista, P. P., & Batista, I. S. (2013). A global view of the atmospheric lunar semidiurnal tide. *Journal of Geophysical Research: Atmosphere*, *118*(23), 13128–13139. https://doi.org/10.1002/2013JD019818

Paulino, A. R., Batista, P. P., Lima, L. M., Clemesha, B. R., Buriti, R. A., & Schuch, N. (2015). The lunar tides in the mesosphere and lower thermosphere over Brazilian sector. *Journal of Atmospheric and Solar-Terrestrial Physics*, *133*, 129–138. https://doi.org/10.1016/j.jastp.2015.08.011

Pedatella, N. M. (2014). Observations and simulations of the ionospheric lunar tide: Seasonal variability. *Journal of Geophysical Research: Space Physics*, *119*(7), 5800–5806. https://doi.org/10.1002/2014JA020189

Pedatella, N. M., & Forbes, J. M. (2010). Evidence for stratosphere sudden warming-ionosphere coupling due to vertically propagating tides. *Geophysical Research Letters*, *37*(11), L11104. https://doi.org/10.1029/2010GL043560

Pedatella, N. M., Liu, H. L., & Richmond, A. D. (2012). Atmospheric semidiurnal lunar tide climatology simulated by the whole atmosphere community climate model. *Journal of Geophysical Research*, *117*(A6), A06327. https://doi.org/10.1029/2012JA017792

Sandford, D. J., Mitchell, N. J., Vincent, R. A., & Murphy, D. J. (2007). The lunar tides in the Antarctic mesosphere and lower thermosphere. *Journal of Atmospheric and Solar-Terrestrial Physics*, *69*(17–18), 2219–2237. https://doi.org/10.1016/j.jastp.2007.04.010

Sandford, D. J., Muller, H. G., & Mitchell, N. J. (2006). Observations of lunar tides in the mesosphere and lower thermosphere at Arctic and middle latitudes. *Atmospheric Chemistry and Physics*, *6*(12), 4117–4127. https://doi.org/10.5194/acp-6-4117-2006

Sathishkumar, S., Sridharan, S., Muhammed Kutty, P. V., & Gurubaran, S. (2017). Long term variabilities and tendencies of mesospheric lunar semidiurnal tide over Tirunelveli (8.7°N, 77.8°E). *Journal of Atmospheric and Solar-Terrestrial Physics*, *163*, 45–53. https://doi.org/10.1016/j.jastp.2017.05.015

Siddiqui, T. A., Stolle, C., Lühr, H., & Matzka, J. (2015). On the relationship between weakening of the northern polar vortex and the lunar tidal amplification in the equatorial electrojet. *Journal of Geophysical Research: Space Physics*, *120*(11), 10006–10019. https://doi.org/10.1002/2015JA021683

Siddiqui, T. A., Yamazaki, Y., Stolle, C., Lühr, H., Matzka, J., Maute, A., & Pedatella, N. (2018). Dependence of lunar tide of the equatorial electrojet on the wintertime polar vortex, solar flux, and QBO. *Geophysical Research Letters*, *45*(9), 3801–3810. https://doi.org/10.1029/2018GL077510

Sridharan, S. (2017). Solar and lunar tidal variabilities in GPS-TEC and geomagnetic field variations: Seasonal as well as during the sudden stratospheric warming of 2010. *Journal of Geophysical Research: Space Physics*, *122*(4), 4571–4587. https://doi.org/10.1002/2016JA023196

Stening, R. J. (2011). Lunar tide in the equatorial electrojet in relation to stratospheric warmings. *Journal of Geophysical Research*, *116*(A12), A12315. https://doi.org/10.1029/2011JA017047

Stening, R. J., Forbes, J. M., Hagan, M. E., & Richmond, A. D. (1997). Experiments with a lunar atmospheric tidal model. *Journal of Geophysical Research*, *102*(D12), 13465–13471. https://doi.org/10.1029/97JD00778

Stening, R. J., Manson, A. H., Meek, C. E., & Vincent, R. A. (1994). Lunar tidal winds at Adelaide and saskatoon at 80 to 100 km heights:1985–1990. *Journal of Geophysical Research*, *99*(A7), 13273–13280. https://doi.org/10.1029/94JA00298

Stening, R. J., Meek, C. E., & Manson, A. H. (1987). Lunar tidal winds measured in the upper-atmosphere (78–105 km) at Saskatoon, Canada. *Journal of the Atmospheric Sciences*, *44*(8), 1143–1151. https://doi.org/10.1175/1520-0469(1987)044<1143:LTWMIT>2.0.CO;2

Stening, R. J., Tsuda, T., & Nakamura, T. (2003). Lunar tidal winds in the upper atmosphere over Jakarta. *Journal of Geophysical Research*, *108*(A5), 1192. https://doi.org/10.1029/2002JA009528

Vial, F., & Forbes, J. M. (1994). Monthly simulations of the lunar semi-diurnal tide. *Journal of Atmospheric and Solar-Terrestrial Physics*, *56*(12), 1591–1607. https://doi.org/10.1016/0021-9169(94)90089-2

von Savigny, C., DeLand, M. T., & Schwartz, M. J. (2017). First identification of lunar tides in satellite observations of noctilucent clouds. *Journal of Atmospheric and Solar-Terrestrial Physics*, *162*, 116–121. https://doi.org/10.1016/j.jastp.2016.07.002

Wu, Q., Ortland, D. A., Killeen, T. L., Roble, R. G., Hagan, M. E., Liu, H.-L., et al. (2008). Global distribution and interannual variations of mesospheric and lower thermospheric neutral wind diurnal tide: 1. Migrating tide. *Journal of Geophysical Research*, *113*(A5), A05308. https://doi.org/10.1029/2007JA012542

Wu, Q., Ward, W., Kristoffersen, S., Maute, A., & Liu, J. (2019). Simulation and observation of lunar tide effect on high-latitude, mesospheric and lower thermospheric winds during the 2013 sudden stratospheric warming event. *Journal of Geophysical Research: Space Physics*, *124*(2), 1283–1291. https://doi.org/10.1029/2018JA025476

Yamazaki, Y., Richmond, A. D., & Yumoto, K. (2012). Stratospheric warmings and the geomagnetic lunar tide: 1958–2007. *Journal of Geophysical Research*, *117*(A4), A04301. https://doi.org/10.1029/2012JA017514

Yamazaki, Y., Stolle, C., Matzka, J., Siddiqui, T. A., Lühr, H., & Alken, P. (2017). Longitudinal variation of the lunar tide in the equatorial electrojet. *Journal of Geophysical Research: Space Physics*, *122*(12), 12445–12463. https://doi.org/10.1002/2017JA024601

Yu, Y., Wan, W., Ning, B., Liu, L., Wang, Z., Hu, L., & Ren, Z. (2013). Tidal wind mapping from observations of a meteor radar chain in December 2011. *Journal of Geophysical Research: Space Physics*, *118*(5), 2321–2332. https://doi.org/10.1029/2012JA017976

Zhang, X., & Forbes, J. M. (2014). Lunar tide in the thermosphere and weakening of the northern polar vortex. *Geophysical Research Letters*, *41*(23), 8201–8207. https://doi.org/10.1002/2014GL062103